International Conference
ENGINEERING MECHANICS 2010
Svratka, Czech Republic, May 10 – 13, 2010

# MODELLING OF BLADED DISK WITH DAMPING EFFECTS IN SLIP SURFACES OF SHROUD

**J. Kellner, V. Zeman, J. Šašek** [1]

**Summary:** *This paper is concentrated on modelling of friction effects in bladed disk of steam turbine, which are realized by means of friction elements placed between blades shroud. The purpose of these elements is to decrease potential high vibrations of bladed disk due to requirement of wide frequency operation range and due to steam flow fluctuations. The model consist of 3D modelled disk and 1D modelled blades. The stiffness coupling matrix and the damping matrix of friction elements effects are obtained by forced vibration of bladed disk, relative movement of adjacent shroud contact areas and by centrifugal forces of friction element.*

## 1. Introduction

The requirements on wide frequency operation range and mainly on higher efficiency of steam turbine blades lead to thinner profile, which is better in term of computation of fluid dynamics (CFD) but blade dynamic properties get worse. The purpose of damping elements is to decrease potential high amplitudes of blade vibration, which may occur due to resonances or big acting forces. The aim of this article is to develop suitable methodology for vibration modelling of damped blades. The method is based on discretization of 3D rotating disk Šašek and Hajžman (2006) and 1D blades Kellner and Zeman (2006) by FEM. This contribution is the rudimentary step for research of dynamic behaviour of the bladed disk with damping elements, which are placed between blade shrouds using the harmonic (balance) linearization method. In future, the damping will be involve due to slip contact interaction in inner couplings between blade shrouds.

## 2. The mathematical modelling of the disk with blade foots

The rotating bladed disk (see fig. 1) can be generally decomposed into a disk (subsystem $D$) and separated blades (subsystems $B_i, i = 1, \ldots, r$). Disk is clamped on inner radius to rigid shaft rotating with constant angular velocity $\omega$ around its $y$ axis. According to the derivation presented in Rao (1989) the disk can be discretized in the rotating $x\ y\ z$ coordinate system using linear isoparametric hexahedral finite elements (see Šašek and Hajžman (2006)). The equation of motion can be written in a configuration space defined by the vector

$$\boldsymbol{q}_D = \left[\ldots, u_j^{(F)}, v_j^{(F)}, w_j^{(F)}, \ldots, u_j^{(C)}, v_j^{(C)}, w_j^{(C)}, \ldots\right]_D^T \in \mathcal{R}^{n_D} \tag{1}$$

[1] Ing. Josef Kellner, Ph.D., Prof. Ing. Vladimír Zeman, DrSc., Ing. Jakub Šašek, Faculty of Applied Sciences, UWB in Pilsen, Univerzitní 22, 306 14 Plzeň, tel. +420 732 556 838, e-mail kennyk@kme.zcu.cz

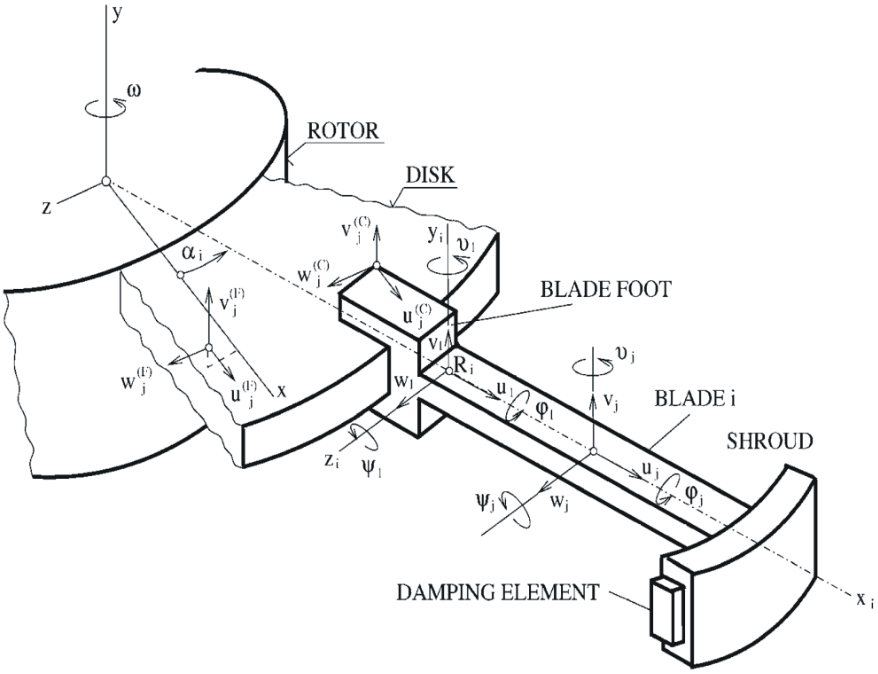


Obrázek 1: Scheme of the rotating bladed disk.

of nodal $j$ displacements (see fig. 1) in direction of rotating axis $x,\ y,\ z$. The disk nodes are classified into free nodes (superscript $F$) and coupled nodes (superscript $C$) on the outer and inner surface of the blade foots. The mathematical model of the disk was derived in Šašek and Hajžman (2006) using Lagrange's equations in the form

$$\boldsymbol{M}_D\ddot{\boldsymbol{q}}_D(t) + \omega\boldsymbol{G}_D\dot{\boldsymbol{q}}_D(t) + \left(\boldsymbol{K}_{sD} - \omega^2\boldsymbol{K}_{dD}\right)\boldsymbol{q}_D(t) = \omega^2\boldsymbol{f}_D\,, \tag{2}$$

where $\boldsymbol{M}_D$, $\boldsymbol{K}_{sD}$ and $\boldsymbol{K}_{dD}$ are symmetric mass, static stiffness and dynamic softening matrices, skew-symmetric matrix $\omega\boldsymbol{G}_D$ expresses gyroscopic effects and $\omega^2\boldsymbol{f}_D$ is force vector of centrifugal load.

The vector of generalized coordinates of the disk can be partitioned according to (1) as

$$\boldsymbol{q}_D = \begin{bmatrix} \boldsymbol{q}_D^{(F)} \\ \boldsymbol{q}_D^{(C)} \end{bmatrix},\ \boldsymbol{q}_D^{(F)} \in \mathcal{R}^{n_D^{(F)}},\ \boldsymbol{q}_D^{(C)} \in \mathcal{R}^{n_D^{(C)}}. \tag{3}$$

The displacements of the coupled disk nodes on condition of rigid blade foots modelled as a disk part can be expressed by displacements of referential nodes $R_i$ which are identical with the first blade nodes $j = 1$ at blade foots (see fig. 1). This relation between coupled disk displacements corresponding to blade $i$ and blade displacements in referential node $R_i$ is

$$\begin{bmatrix} u_j^{(C)} \\ v_j^{(C)} \\ w_j^{(C)} \end{bmatrix} = \begin{bmatrix} \cos\alpha_i & 0 & \sin\alpha_i \\ 0 & 1 & 0 \\ -\sin\alpha_i & 0 & \cos\alpha_i \end{bmatrix} \left[\begin{array}{ccc|ccc} 1 & 0 & 0 & 0 & z_j & -y_j \\ 0 & 1 & 0 & -z_j & 0 & x_j \\ 0 & 0 & 1 & y_j & -x_j & 0 \end{array}\right] \begin{bmatrix} u_1 \\ v_1 \\ w_1 \\ \varphi_1 \\ \vartheta_1 \\ \psi_1 \end{bmatrix}_{B,i}, \tag{4}$$

or shortly

$$\boldsymbol{q}_j^{(C)} = \boldsymbol{T}_{\alpha_i} \boldsymbol{T}_j \boldsymbol{q}_{1,i}, \qquad i = 1, 2, \ldots, r, \tag{5}$$

where $x_j,\ y_j,\ z_j$ are coordinates of the coupled disk node $j$ on the rigid blade foots in coordinate system $x_i,\ y_i,\ z_i$ of the blade $i$ with the origin in the first blade node and $\alpha_i$ is the angle between the rotating disk axis $x$ and the rotating blade axis $x_i$. Coordinates of vector $\boldsymbol{q}_{1,i}$ express the referential node displacements in direction of blade rotating axes $x_i, y_i, z_i$ and small turn angles of the blade cross section in node $R_i$.

The complete transformation between displacements of coupled nodes of the disk on the blade foots and the referential nodes $R_i$ of all blades can be expressed in the matrix form

$$\left[\begin{array}{c} \vdots \\ \hline \boldsymbol{q}_j^{(C)} \\ \hline \vdots \end{array}\right] = \left[\begin{array}{c|c|c} & \vdots & \\ \hline \ldots & \boldsymbol{T}_{\alpha_i}\boldsymbol{T}_j & \ldots \\ \hline & \vdots & \end{array}\right] \left[\begin{array}{c} \vdots \\ \hline \boldsymbol{q}_{1,i} \\ \hline \vdots \end{array}\right] \Rightarrow \boldsymbol{q}_D^{(C)} = \boldsymbol{T}_{D,R} \boldsymbol{q}_R. \tag{6}$$

The global transformation rectangular matrix $\boldsymbol{T}_{D,R} \in \mathcal{R}^{n_D^{(C)}, n_R}$ describes the linkage between the disk ($D$) and the blade rim ($R$). Coordinates of vector $\boldsymbol{q}_R$ express displacements of the blade nodes $j = 1,\ 2,\ \ldots, N$ (see below) in coordinate systems $x_i,\ y_i,\ z_i$ (see fig. 1) in order of blades (for $i = 1,\ 2, \ldots, r$)

$$\boldsymbol{q}_R = \left[\boldsymbol{q}_{B,1}^T \quad \boldsymbol{q}_{B,2}^T \quad \ldots \boldsymbol{q}_{B,r}^T\right]^T \in \mathcal{R}^{n_R}, \qquad , n_R = 6Nr, \tag{7}$$

where $r$ is the blade number.

For illustration we present in table 1a number of lowest natural frequencies of the nonrotating centrally clamped modeled disk (see fig. 2) with rigid blade foots but without blades. The nodes which lie on the inner radius are fixed in all directions. The mode shapes corresponding to natural frequencies are characterized by the number of nodal diameters (ND) and the number of nodal circles (NC). the modal values of the disk with foots modelled as flexible differ from the disk model with rigid foots very small Zeman et al., (2009).

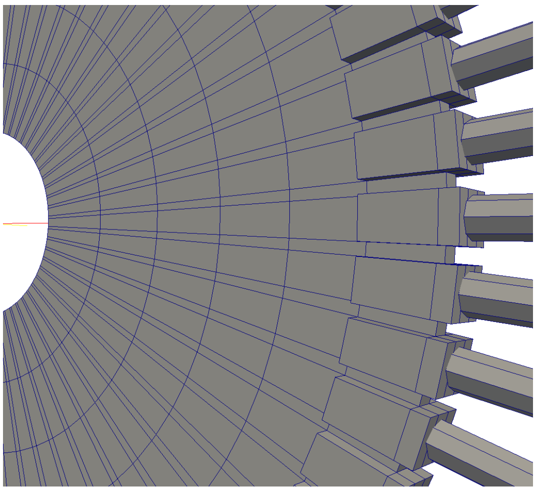

Obrázek 2: Scheme of the disk with blade foots.

| Frequencies of disk with blade foots | | |
|---|---|---|
| | [Hz] | shape |
| 1 | 234,8 | 1 ND |
| 2 | 234,8 | 1 ND |
| 3 | 249,8 | 1 NC |
| 4 | 306,7 | 2 ND |
| 5 | 306,7 | 2 ND |
| 6 | 599,3 | 3 ND |
| 7 | 599,3 | 3 ND |

Tabulka 1: Modal analysis of the disk with rigid blade foots.

## 3. The blade rim with damping elements in shroud – contact stiffness

The single blades are modelled as one dimensional continuum linked with rigid shroud body in its centre of gravity of last blade profile. The mathematical model of the uncoupled blade $i$ with shroud in configuration space of its blade node displacements (in the direction of rotating axes $x_i,\ y_i,\ z_i$ and of small angular displacements of the blade cross sections)

$$\boldsymbol{q}_{B,i} = [\ldots, u_j, v_j, w_j, \varphi_j, \vartheta_j, \psi_j, \ldots]^T_{B,i} \in \mathcal{R}^{n_B},\ i = 1, 2, \ldots, r; j = 1, 2, \ldots, N \qquad (8)$$

has the form Kellner and Zeman (2006), Kellner (2009)

$$\boldsymbol{M}_B \ddot{\boldsymbol{q}}_{B,i}(t) + \omega \boldsymbol{G}_B \dot{\boldsymbol{q}}_{B,i}(t) + \left(\boldsymbol{K}_{sB} + \omega^2 \boldsymbol{K}_{\omega B} - \omega^2 \boldsymbol{K}_{dB}\right) \boldsymbol{q}_{B,i}(t) = \omega^2 \boldsymbol{f}_B\,, \qquad (9)$$

where blade matrices $\boldsymbol{M}_B$, $\boldsymbol{K}_{sB}$, $\boldsymbol{K}_{dB}$ and $\boldsymbol{G}_B$ have an identical meaning with matrices of the disk and matrix $\omega^2 \boldsymbol{K}_{\omega,B}$ expresses a centrifugal blade stiffening.

In this first modelling task is supposed, that the damping element is fast connected on the sloping side with blade $i+1$ because the frictional force here is much higher than on the straight (radial) side of the damping element. This model in the first step of modelling respects only a contact stiffness between blade $i$ and damping element connected with following blade $i+1$ on the radial area. This contact stiffness is defined by contact stiffness matrix between blades $i$ and $i+1$

$$\mathbf{K}_C^{(B)} = diag\,(0 \quad 0 \quad k_\zeta \quad k_{\xi\xi} \quad k_{\eta\eta} \quad 0)_{\xi_i,\eta_i,\zeta_i}\,, \qquad (10)$$

expressing the constraint for the circumferential displacement and two rotations by means of contact stiffness $k_\zeta$ in normal direction to radial area $\xi_i\eta_i$ and two flexural stiffnesses $k_{\xi\xi},\ k_{\eta\eta}$ .

This contact stiffness matrix is expressed in local contact coordinate system $\xi_i, \eta_i, \zeta_i$ placed in central contact point $B_i$ of the $i$-th blade shroud. The coupling (deformation) energy between two adjacent blades $i$ and $i+1$ (see fig. 3) is, in this contact coordinate system, expressed as

$$E_C^{i,i+1} = \frac{1}{2}\left(\boldsymbol{q}_{B_i} - \boldsymbol{q}_{A_{i+1}}\right)^T_{\xi_i,\eta_i,\zeta_i} \mathbf{K}_C^{(B)} \left(\boldsymbol{q}_{B_i} - \boldsymbol{q}_{A_{i+1}}\right)_{\xi_i,\eta_i,\zeta_i}\,, \qquad (11)$$

where $\boldsymbol{q}_{B_i}, \boldsymbol{q}_{A_{i+1}}$ are vectors of blade $i$ displacements in point $B_i$ and blade $i+1$ displacements in point$A_{i+1}$ expressed in coordinate system $\xi_i, \eta_i, \zeta_i$. The difference between $\boldsymbol{q}_{B_i} - \boldsymbol{q}_{A_{i+1}}$ represents the relative motion of contact areas between two adjacent blades $i$ and $i+1$.

The translation of blade local coordinate systems from point $C_i$ to point $B_i$ and from point $C_{i+1}$ to point $A_{i+1}$ is expressed by translation matrices

$$\boldsymbol{R}_X^T = \begin{bmatrix} 0 & z_X & -y_X \\ -z_X & 0 & x_X \\ y_X & -x_X & 0 \end{bmatrix}, \quad X = A_{i+1}, B_i. \tag{12}$$

The translated local coordinate system is then rotated so, that the contact coordinate axis $\xi_i$ is the radial according to bladed disk axis of rotation $y_f$.

The vector of displacements in point $B_i$ in the contact coordinate system is

$$\boldsymbol{q}_{B_i\ \xi_i,\eta_i,\zeta_i} = \begin{bmatrix} u_{B_i} \\ v_{B_i} \\ w_{B_i} \\ \varphi_{B_i} \\ \vartheta_{B_i} \\ \psi_{B_i} \end{bmatrix}_{\xi_i,\eta_i,\zeta_i} = \left[\begin{array}{c|c} \boldsymbol{\tau}_B & \mathbf{0} \\ \hline \mathbf{0} & \boldsymbol{\tau}_B \end{array}\right] \left.\begin{matrix} \left.\begin{bmatrix} u_{B_i} \\ v_{B_i} \\ w_{B_i} \end{bmatrix}\right\} \mathbf{u}_{B_i} \\ \left.\begin{bmatrix} \varphi_{B_i} \\ \vartheta_{B_i} \\ \psi_{B_i} \end{bmatrix}_{x_i,z_i,y_i}\right\} \boldsymbol{\varphi}_{B_i} \end{matrix}\right\} \boldsymbol{q}_{B_i\ x_i,y_i,z_i}, \tag{13}$$

where the rotation matrix $\boldsymbol{\tau}_B$ between coordinate systems is specified by angle $\delta_B$ between radial axis $x_i$ of blade passing through point $C_i$ and radial axis $\xi_i$ passing through point $B_i$.

$$\boldsymbol{\tau}_B = \begin{bmatrix} \cos\delta_B & 0 & -\sin\delta_B \\ 0 & 1 & 0 \\ \sin\delta_B & 0 & \cos\delta_B \end{bmatrix}. \tag{14}$$

Analogously the vector of displacements of point $A_{i+1}$ in this contact coordinate system is

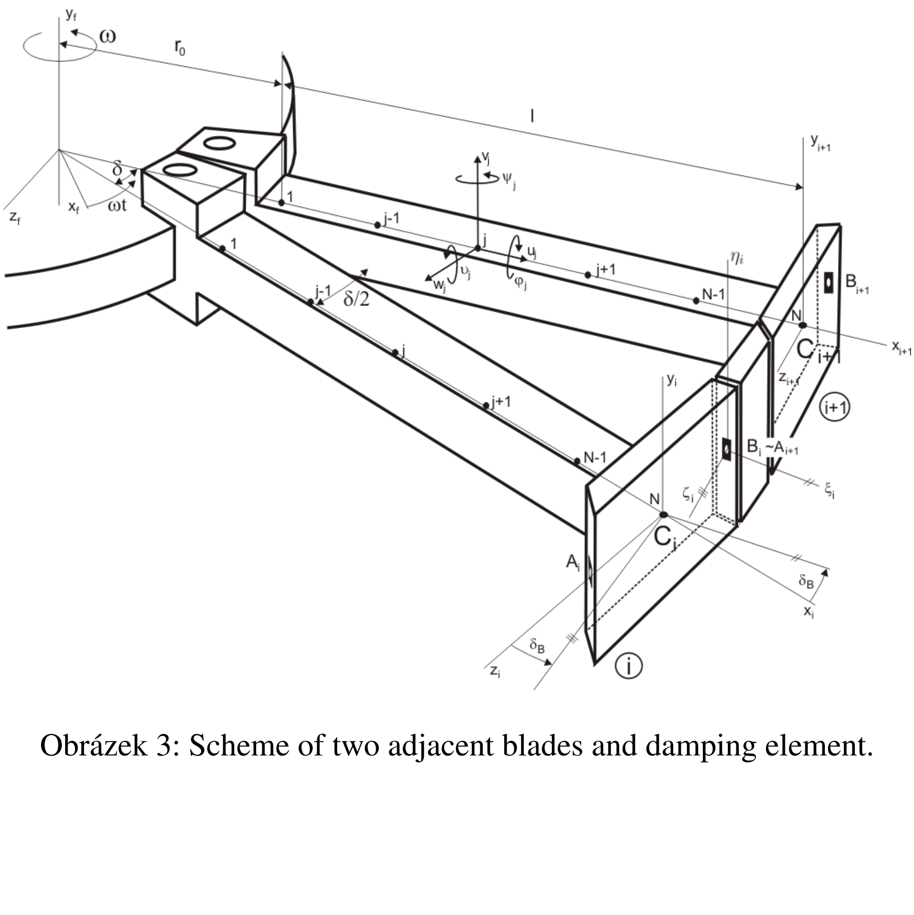


Obrázek 3: Scheme of two adjacent blades and damping element.

defined as

$$\boldsymbol{q}_{A_{i+1}\ \xi_i,\eta_i,\zeta_i} = \begin{bmatrix} \boldsymbol{\tau}_A & \mathbf{0} \\ \mathbf{0} & \boldsymbol{\tau}_A \end{bmatrix} \boldsymbol{q}_{A_{i+1}\ x_{i+1},y_{i+1},z_{i+1}}, \tag{15}$$

where

$$\boldsymbol{\tau}_A = \begin{bmatrix} \cos\delta_A & 0 & \sin\delta_A \\ 0 & 1 & 0 \\ -\sin\delta_A & 0 & \cos\delta_A \end{bmatrix}. \tag{16}$$

The vector of blade $i$ displacements in point $B_i$ in coordinate system $x_i, y_i, z_i$ is defined by generalized displacements of point $C_i$ and by matrix of translation $\boldsymbol{R}_B$

$$\boldsymbol{q}_{B_i\ x_i,y_i,z_i} = \begin{bmatrix} \boldsymbol{u}_{B_i} \\ \boldsymbol{\varphi}_{B_i} \end{bmatrix}_{x_i,y_i,z_i} = \begin{bmatrix} \boldsymbol{E} & \boldsymbol{R}_B^T \\ \mathbf{0} & \boldsymbol{E} \end{bmatrix} \begin{bmatrix} \boldsymbol{u}_{C_i} \\ \boldsymbol{\varphi}_{C_i} \end{bmatrix}_{x_i,y_i,z_i} = \begin{bmatrix} \boldsymbol{E} & \boldsymbol{R}_B^T \\ \mathbf{0} & \boldsymbol{E} \end{bmatrix} \boldsymbol{q}_{C_i}. \tag{17}$$

According to (13) this vector in the contact coordinate system $\xi_i, \eta_i, \zeta_i$ has the form

$$\boldsymbol{q}_{B_i\ \xi_i,\eta_i,\zeta_i} = \underbrace{\begin{bmatrix} \boldsymbol{\tau_B} & \mathbf{0} \\ \mathbf{0} & \boldsymbol{\tau}_B \end{bmatrix} \begin{bmatrix} \boldsymbol{E} & \boldsymbol{R}_B^T \\ \mathbf{0} & \boldsymbol{E} \end{bmatrix}}_{\boldsymbol{T}_B} \boldsymbol{q}_{C_i\ x_i,y_i,z_i}. \tag{18}$$

Analogously, the vector of blade $i+1$ displacements in point $A_{i+1}$ in the contact coordinate system $\xi_i, \eta_i, \zeta_i$ is expressed as

$$\boldsymbol{q}_{A_{i+1}\ \xi_i,\eta_i,\zeta_i} = \underbrace{\begin{bmatrix} \boldsymbol{\tau_A} & \mathbf{0} \\ \mathbf{0} & \boldsymbol{\tau}_A \end{bmatrix} \begin{bmatrix} \boldsymbol{E} & \boldsymbol{R}_A^T \\ \mathbf{0} & \boldsymbol{E} \end{bmatrix}}_{\boldsymbol{T}_A} \boldsymbol{q}_{C_{i+1}\ x_{i+1},y_{i+1},z_{i+1}}. \tag{19}$$

We can now express the coupling energy, defined in (11)by means of generalized coordinates of $i$-th and $i+1$-th blades in the form

$$E_C^{i,i+1} = \frac{1}{2}\left(\boldsymbol{T}_B\boldsymbol{q}_{C_i} - \boldsymbol{T}_A\boldsymbol{q}_{C_{i+1}}\right)^T \mathbf{K}_C^{(B)} \left(\boldsymbol{T}_B\boldsymbol{q}_{C_i} - \boldsymbol{T}_A\boldsymbol{q}_{C_{i+1}}\right). \tag{20}$$

After multiplying the previous equation and from identity $\frac{\partial E_C^{i,i+1}}{\partial \boldsymbol{q}_R} = \boldsymbol{K}_{C_i}^{(R)}\boldsymbol{q}_R$ we obtain the stiffness matrix of coupling between two adjacent blades $i$ and $i+1$ in the form

$$\mathbf{K}_{C_i}^{(R)} = \begin{array}{c} \begin{array}{ccccc} & \boldsymbol{q}_{C_i}^T & & \boldsymbol{q}_{C_{i+1}}^T & \end{array} \\ \left[\begin{array}{c|c|c|c|c} \vdots & & \vdots & & \vdots \\ \hline \cdots & \overbrace{\mathbf{T}_B^T\mathbf{K}_C^{(B)}\mathbf{T}_B}^{\mathbf{K}_{B,B}} & \cdots & \overbrace{-\mathbf{T}_B^T\mathbf{K}_C^{(B)}\mathbf{T}_A}^{-\mathbf{K}_{B,A}} & \cdots \\ \hline \vdots & & \vdots & & \vdots \\ \hline \cdots & \overbrace{-\mathbf{T}_A^T\mathbf{K}_C^{(B)}\mathbf{T}_B}^{-\mathbf{K}_{A,B}} & \cdots & \overbrace{\mathbf{T}_A^T\mathbf{K}_C^{(B)}\mathbf{T}_A}^{\mathbf{K}_{A,A}} & \cdots \\ \hline \vdots & & \vdots & & \vdots \end{array}\right] \end{array} \begin{array}{l} \\ \left.\begin{array}{l} \\ \boldsymbol{q}_{C_i} \\ \end{array}\right\} \boldsymbol{q}_{B,i} \\ \left.\begin{array}{l} \\ \boldsymbol{q}_{C_{i+1}} \\ \end{array}\right\} \boldsymbol{q}_{B,i+1} \end{array}, \tag{21}$$

where $\boldsymbol{q}_{B,i}$ and $\boldsymbol{q}_{B,i+1}$ are the vectors of all generalized displacements of blade $i$ and $i$-th. Vectors $\boldsymbol{q}_{C_i}$ and $\boldsymbol{q}_{C,i+1}$ are the vectors of generalized displacements in the last node $N$ on blade $i$ and $i$-th, respectively.

The whole coupling stiffness matrix between all blades (here 60 blades) is then

$$
\mathbf{K}_C^{(R)} = \begin{array}{c}
\begin{array}{cccccccccc}
 & \boldsymbol{q}_{C_1}^T & & \boldsymbol{q}_{C_2}^T & & \boldsymbol{q}_{C_3}^T & & \boldsymbol{q}_{C_{59}}^T & & \boldsymbol{q}_{C_{60}}^T
\end{array} \\
\left[\begin{array}{c|c|c|c|c|c|c|c|c|c}
\vdots & & \vdots & & \vdots & & \vdots & & \vdots & \\ \hline
\cdots & \mathbf{K}_{A,A}+\mathbf{K}_{B,B} & \cdots & -\mathbf{K}_{B,A} & \cdots & & \cdots & & \cdots & -\mathbf{K}_{A,B} \\ \hline
\vdots & & \vdots & & \vdots & & \vdots & & \vdots & \\ \hline
\cdots & -\mathbf{K}_{A,B} & \cdots & \mathbf{K}_{A,A}+\mathbf{K}_{B,B} & \cdots & -\mathbf{K}_{B,A} & \cdots & & \cdots & \\ \hline
\vdots & & \vdots & & \vdots & & \vdots & & \vdots & \\ \hline
\cdots & & \cdots & -\mathbf{K}_{A,B} & \cdots & \mathbf{K}_{A,A}+\mathbf{K}_{B,B} & \cdots & -\mathbf{K}_{B,A} & & \\ \hline
\approx & \approx & \approx & \approx & \approx & \approx & \approx & \approx & \approx & \approx \\
\approx & \approx & \approx & \approx & \approx & \approx & \approx & \approx & \approx & \approx \\ \hline
\vdots & & \vdots & & \vdots & & \vdots & & \vdots & \\ \hline
\cdots & & \cdots & & \cdots & & \cdots & \mathbf{K}_{A,A}+\mathbf{K}_{B,B} & \cdots & -\mathbf{K}_{B,A} \\ \hline
\vdots & & \vdots & & \vdots & & \vdots & & \vdots & \\ \hline
\cdots & -\mathbf{K}_{B,A} & \cdots & & \cdots & & \cdots & -\mathbf{K}_{A,B} & & \mathbf{K}_{A,A}+\mathbf{K}_{B,B}
\end{array}\right]
\end{array} . \tag{22}
$$

This contact stiffness matrix connects the blades together into a blade rim, whose equation of motion is

$$\boldsymbol{M}_R\ddot{\boldsymbol{q}}_R(t) + \omega\boldsymbol{G}_R\dot{\boldsymbol{q}}_R(t) + \left(\boldsymbol{K}_{sR} + \boldsymbol{K}_C^{(R)} + \omega^2\boldsymbol{K}_{\omega R} - \omega^2\boldsymbol{K}_{dR}\right)\boldsymbol{q}_R(t) = \omega^2\boldsymbol{f}_R\,, \tag{23}$$

where all matrices (except $\boldsymbol{K}_C^{(R)}$ are block-diagonal in the form

$$\boldsymbol{X}_R = diag\left(\boldsymbol{X}_B,\, \boldsymbol{X}_B,\, \ldots,\, \boldsymbol{X}_B\right), \quad \boldsymbol{X} = \boldsymbol{M}, \boldsymbol{G}, \boldsymbol{K}_s, \boldsymbol{M}_d, \boldsymbol{K}_\omega, \boldsymbol{f}. \tag{24}$$

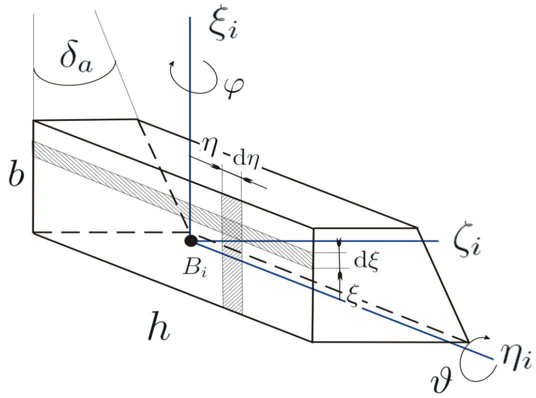


Obrázek 4: Scheme of the damping element.

The contact stiffness matrix $\boldsymbol{K}_C^{(B)}$ defined in (10) depends on geometric and material characteristics of damping element. Mentioned above, the frictional force is much higher on the slopping side, so at the first time the damping element is considered fast connect here. The normal force in the contact on radial straight side is

$$N_0 = \frac{m_T r\omega^2}{\tan\delta_\alpha}, \tag{25}$$

where $m_T$ is the damping element mass, $\omega = \frac{\pi n}{30}$ is the angular velocity and $r$ is radius of damping element centre of gravity. The contact stress is

$$\sigma_{[MPa]} = \frac{N_{0\,[N]}}{A_{ef\,[mm^2]}}, \quad A_{ef} = \overbrace{h\gamma_h}^{h_{ef}}\overbrace{b\gamma_b}^{b_{ef}}.10^6 \tag{26}$$

where $h$ is axial and $b$ is radial damping element proportions and $A_{ef}$ is the effective contact area (see fig. 4), defined by real size of contact area, i.e. the high $h$ multiply by coefficient $\gamma_h$ etc.

The contact normal stiffness in direction $\zeta$ is

$$k_\zeta = \frac{N_0}{\delta}.10^6 [N/m], \tag{27}$$

where contact deformation $\delta_{[\mu m]} = c\sigma^p$ in $\mu m$ is defined, according to Riwin (1999), by contact deformation coefficient $c$ and contact exponent $p$. Moments of flexion around axes $\xi_i$ and $\eta_i$ can be expressed as

$$M_\xi = 2\int_0^{h_{ef}/2} k_I b_{ef} \mathrm{d}\eta\, \eta^2 \varphi = \frac{1}{12} \underbrace{k_I b_{ef} h_{ef}}_{k_\zeta} h_{ef}^2 \varphi,$$
$$M_\eta = 2\int_0^{b_{ef}/2} k_I h_{ef} \mathrm{d}\xi\, \xi^2 \varphi = \frac{1}{12} \underbrace{k_I b_{ef} h_{ef}}_{k_\zeta} b_{ef}^2 \varphi, \tag{28}$$

where unit contact stiffness $k_I$ is supposed constant and the angles of relative turning of interface surfaces are marked as $\varphi$ and $\vartheta$. Two flexural contact stiffnesses are then

$$k_{\xi\xi} = \frac{1}{12} k_\zeta \left(h\gamma_h\right)^2, \qquad k_{\eta\eta} = \frac{1}{12} k_\zeta \left(b\gamma_b\right)^2. \tag{29}$$

## 4. The modelling of bladed disk with damping elements in blade shroud

The motion equations of the fictive undamped system assembled from uncoupled subsystems – the central clamped disk with rigid blade roots and blade rim with damping elements in shroud – in the configuration space

$$\boldsymbol{q} = \left[\left(\boldsymbol{q}_D^{(F)}\right)^T \left(\boldsymbol{q}_D^{(C)}\right)^T \boldsymbol{q}_R^T\right]^T \tag{30}$$

can be formally rewritten as

$$\boldsymbol{M}\ddot{\boldsymbol{q}}(t) + \omega\boldsymbol{G}\dot{\boldsymbol{q}}(t) + \left(\boldsymbol{K}_s + \omega^2\boldsymbol{K}_\omega - \omega^2\boldsymbol{K}_d\right)\boldsymbol{q}(t) = \omega^2\boldsymbol{f}. \tag{31}$$

According to mathematical models (2) and (23), all matrices have the block-diagonal form

$$\boldsymbol{X} = diag\left(\boldsymbol{X}_D,\ \boldsymbol{X}_R\right),\ \boldsymbol{X} = \boldsymbol{M},\ \boldsymbol{G},\ \boldsymbol{K}_d,$$
$$\boldsymbol{K}_s = diag(\boldsymbol{K}_{sD},\ \boldsymbol{K}_{sR} + \boldsymbol{K}_C^{(R)}),\ \boldsymbol{K}_\omega = diag(\boldsymbol{0},\ \boldsymbol{K}_{\omega R}) \tag{32}$$

and $\boldsymbol{f} = \left[\boldsymbol{f}_D^T,\ \boldsymbol{f}_R^T\right]^T$. The vector of generalized coordinates $\boldsymbol{q}(t)$ of the real bladed disk in consequence of the couplings (6) can be transformed into new vector $\tilde{\boldsymbol{q}}$ in the form

$$\begin{bmatrix} \boldsymbol{q}_D^{(F)} \\ \boldsymbol{q}_D^{(C)} \\ \boldsymbol{q}_R \end{bmatrix} = \begin{bmatrix} \boldsymbol{E} & \boldsymbol{0} \\ \boldsymbol{0} & \boldsymbol{T}_{D,R} \\ \boldsymbol{0} & \boldsymbol{E} \end{bmatrix} \begin{bmatrix} \boldsymbol{q}_D^{(F)} \\ \boldsymbol{q}_R \end{bmatrix} \text{ or shortly } \boldsymbol{q} = \boldsymbol{T}\tilde{\boldsymbol{q}}. \tag{33}$$

The mathematical model of the central clamped bladed disk with damping elements in blade shroud in the configuration space $\tilde{\boldsymbol{q}}$ takes the form

$$\tilde{\boldsymbol{M}}\ddot{\tilde{\boldsymbol{q}}}(t) + \omega\tilde{\boldsymbol{G}}\dot{\tilde{\boldsymbol{q}}}(t) + \left(\tilde{\boldsymbol{K}}_s + \omega^2\tilde{\boldsymbol{K}}_\omega - \omega^2\tilde{\boldsymbol{K}}_d\right)\tilde{\boldsymbol{q}}(t) = \omega^2\tilde{\boldsymbol{f}}, \tag{34}$$

where $\tilde{\boldsymbol{X}} = \boldsymbol{T}^T\boldsymbol{X}\boldsymbol{T}$, $\boldsymbol{X} = \boldsymbol{M}, \boldsymbol{G}, \boldsymbol{K}_s, \boldsymbol{K}_d, \boldsymbol{K}_\omega$ and $\tilde{\boldsymbol{f}} = \boldsymbol{T}^T\boldsymbol{f}$.

## 5. Modal analysis of bladed disk

The results of blade and shrouded blade modelling was compared with results from commercial software ANSYS. For illustration we present in tab. 2 a number of lowest natural frequencies of the one modeled blade with shroud fixed in the first node on the rigid disk with rigid blade roots. The DOF number of 1D blade model is 36 without reduction (see fig. 5). The first and second natural frequencies are sufficiently accurate, moreover the influence of rotation is practically same also for higher frequencies.

Tabulka 2: Modal analysis of the blade with shroud in different FEM softwares.

| Frequencies of blade with shroud | | | |
|---|---|---|---|
| **ANSYS** | **MATLAB** | **ANSYS** | **MATLAB** |
| 0 rpm | | 2000 rpm | |
| 142 | 141 | 153 | 151 |
| 282 | 282 | 288 | 286 |
| 970,5 | 1003 | 981,5 | 1011 |
| 1536 | 1533 | 1537 | 1533 |
| 1907 | 1969 | 1913 | 1974 |

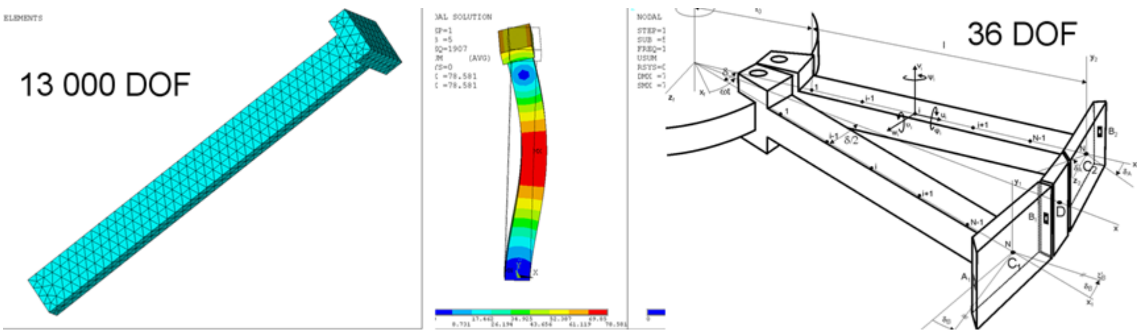


Obrázek 5: Model in Ansys (left picture) and model scheme in MATLAB (right picture).

The next step of the testing of the presented method was modal analysis of blade rim, i.e. the blades with shroud connected by contact stiffness matrix $\boldsymbol{K}_R^{(C)}$ of damping elements.The results of modal analysis in the form of the some few lowest natural frequencies of the the blade rim fixed in the first nodes of all blades into rigid disk with rigid blade roots are presented in tab. 3.

All blades of the blade rim with damping elements are connected with disk rigid foots in the first nodes and the mathematical model (34) of the bladed disk is used for testing. Its modal analysis is performed for undermentioned parameters:

Tabulka 3: Modal analysis of the blade rim.

| Frequencies of blade rim | | | |
|---|---|---|---|
| Fixed in 1st nodes of blades | | Fixed in 1st nodes of blades | |
| 0 rpm | | 2000 rpm | |
| [Hz] | number | [Hz] | number |
| 142 | 60x | 151 | 60x |
| 291 | 1x | 295 | 1x |
| 618 | 2x | 620 | 2x |
| 1003 | 60x | 1011 | 60x |
| 1068 | 2x | 1069 | 2x |
| 1390 | 2x | 1392 | 2x |

$\delta_a$ = 20° (angle of damping element slope)
$\delta_A$ = 3.45° (angle between radial blade axis $x_{i+1}$ and axis $\xi_i$)
$\delta_B$ = 2.55° (angle between radial blade axis $x_i$ and axis $\xi_i$)
$m_T$ = 0.0086 kg (mass of damping element)
$r_T$ = 0.4655 m (distance of the centre of gravity of damping element from the rotation axis)
$c$ = 3 (contact deformation coefficient )
$p$ = 0.5 (contact exponent)
$b$ = 0.006 m (radial proportion of damping element)
$h$ = 0.02 m (axial proportion of damping element)
$\gamma_b$ = 0.5 (coefficient of contact area reduction in radial proportion)
$\gamma_h$ = 0.5 (coefficient of contact area reduction in axial direction).

The some few lowest natural frequencies of the central clamped blade disk with damping elements in the blade shroud are presented in tab. 4. The corresponding mode shapes are characterized by the number of nodal diameters $ND$ and nodal circles $NC$, i.e. the number of lines (resp. circles) with zero amplitude. The graphic demonstration of mode shapes is available but in this paper in gray-scale there are presented for illustration only chosen shapes depicted without shroud and damping elements (see fig. 6 - 7).

Tabulka 4: Eigenfrequencies of bladed disk - clamped on inner radius.

| Frequencies of bladed disk Clamped in inner disk radius | | | | | |
|---|---|---|---|---|---|
| 0 rpm | | | 2000 rpm | | |
| [Hz] | number | shape | [Hz] | number | shape |
| 69,5 | 2x | 1 ND | 75,9 | 2 | 1 ND |
| 71,7 | 1x | 1 NC | 78,3 | 1 | 1 NC |
| 84,6 | 2x | 2 ND | 91,2 | 2 | 2 ND |
| 113,2 | 2x | 3 ND | 121,8 | 2 | 3 ND |
| 125,5 | 2x | 4 ND | 135,0 | 2 | 4 ND |
| 130,1 | 2x | 5 ND | 140,0 | 2 | 5 ND |

## 6. Damping effects in slip surfaces on shroud

Previously mentioned, the damping element is in this paper fast connected on the slope contact area and the friction effects are realized only on the radial side of the damping element. The

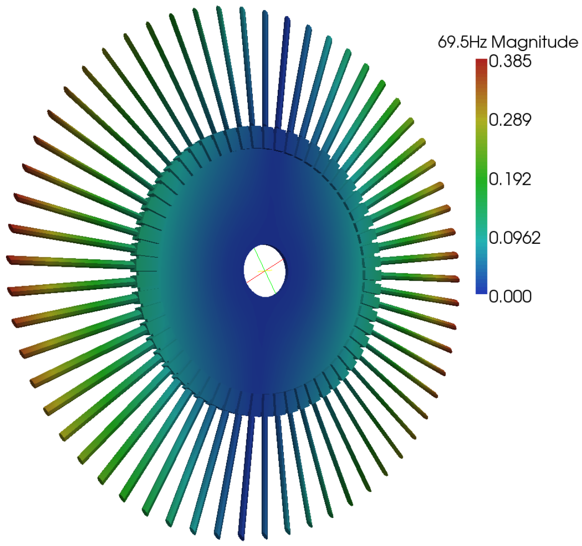


Obrázek 6: Mode shape corresponding to eigenfrequency 69,5 Hz - 1 ND for non-rotating bladed disk.

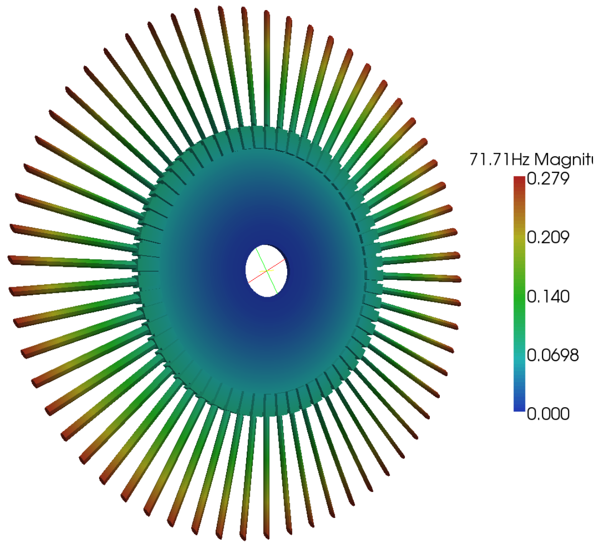


Obrázek 7: Mode shape corresponding to eigenfrequency 71,7 Hz - 0 ND for non-rotating bladed disk.

relative movement of opposite contact areas (the radial side of $i$-th element and the contact area of the adjacent blade shroud) is characterized by an ellipse in $\widehat{\eta_i \xi_i}$ plane (fig. 4) and can be turned by an angle $\alpha_i$ (fig. 8), the ellipse axes of this movement are $a_i$, $b_i$. The matrix $\boldsymbol{B}_{e_i} = diag(b_{\grave{\xi}_i}, b_{\grave{\eta}_i}, b_{\grave{\Phi}_i})$ is an equivalent damping matrix of friction forces between $i$-th blade damping element and adjacent shroud. This matrix is defined in local coordinate system $\grave{\xi}_i \grave{\eta}_i \grave{\zeta}_i$ connected with axes of movement ellipse (fig. 9).

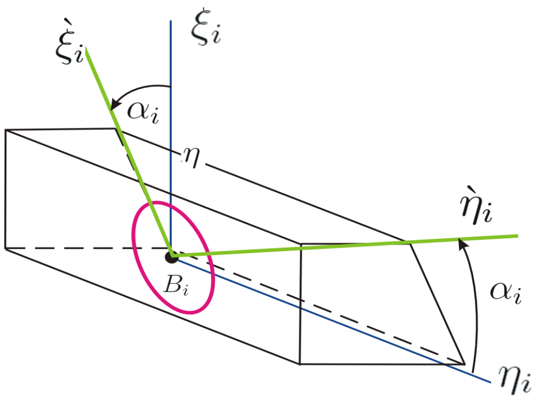


Obrázek 8: Relative displacements between the damping element and adjacent shroud during one period of excitation.

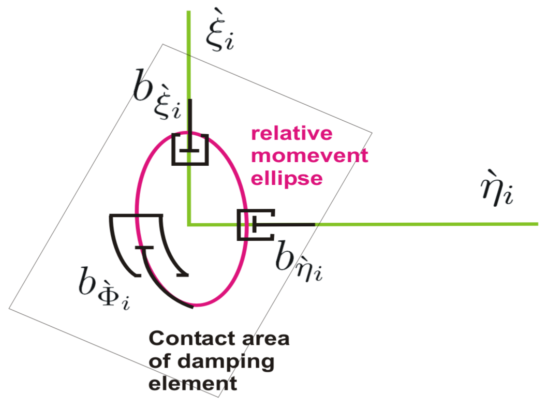


Obrázek 9: Graphical interpreting of dampers placed in axes of relative movement ellipse..

The vector of relative slip velocities defined in contact plane $\widehat{\eta_i \xi_i}$ between $i$-th and $i+1$-th blades is

$$\boldsymbol{c}_i = \begin{bmatrix} c_{\xi_i} \\ c_{\eta_i} \\ c_{\Phi_i} \end{bmatrix} = \begin{bmatrix} \boldsymbol{\xi}_B^T \\ \boldsymbol{\eta}_B^T \\ \boldsymbol{\zeta}_B^T \end{bmatrix} \dot{\boldsymbol{q}}_{C_i} - \begin{bmatrix} \boldsymbol{\xi}_A^T \\ \boldsymbol{\eta}_A^T \\ \boldsymbol{\zeta}_A^T \end{bmatrix} \dot{\boldsymbol{q}}_{C_{i+1}} = \boldsymbol{\tau}_{FB} \dot{\boldsymbol{q}}_{C_i} - \boldsymbol{\tau}_{FA} \dot{\boldsymbol{q}}_{C_{i+1}}. \tag{35}$$

The transformation matrices $\boldsymbol{\tau}_{FA}$ and $\boldsymbol{\tau}_{FB}$ are in the form

$$\boldsymbol{\tau}_{FA} = \begin{bmatrix} \cos\delta_A & 0 & \sin\delta_A & 0 & \cos\delta_A z_A - \sin\delta_A x_A & 0 \\ 0 & 1 & 0 & -z_A & 0 & x_A \\ 0 & 0 & 0 & -\sin\delta_A & 0 & \cos\delta_A \end{bmatrix} = \begin{bmatrix} \boldsymbol{\xi}_A^T \\ \boldsymbol{\eta}_A^T \\ \boldsymbol{\zeta}_A^T \end{bmatrix}, \tag{36}$$

$$\boldsymbol{\tau}_{FB} = \begin{bmatrix} \cos\delta_B & 0 & -\sin\delta_B & 0 & \cos\delta_B z_B & 0 \\ 0 & 1 & 0 & -z_B & 0 & 0 \\ 0 & 0 & 0 & \sin\delta_B & 0 & \cos\delta_B \end{bmatrix} = \begin{bmatrix} \boldsymbol{\xi}_B^T \\ \boldsymbol{\eta}_B^T \\ \boldsymbol{\zeta}_B^T \end{bmatrix}. \tag{37}$$

Because the calculation of $\boldsymbol{B}_i$ must be done in the coordinate system connected with axes of movement ellipse, the vector of slip velocities defined in this revolved contact plane $\widehat{\grave{\eta}_i\grave{\xi}_i}$ is

$$\grave{\boldsymbol{c}}_i = \begin{bmatrix} \grave{c}_{\xi_i} \\ \grave{c}_{\eta_i} \\ \grave{c}_{\Phi_i} \end{bmatrix} = \begin{bmatrix} \cos\alpha_i & \sin\alpha_i & 0 \\ -\sin\alpha_i & \cos\alpha_i & 0 \\ 0 & 0 & 1 \end{bmatrix} \begin{bmatrix} c_{\xi_i} \\ c_{\eta_i} \\ c_{\Phi_i} \end{bmatrix} = \boldsymbol{\tau}_{\alpha_i}\boldsymbol{c}_i. \tag{38}$$

The dissipation function of friction effects in $i$-th contact area is by using the equivalent damping (defined by method of equivalent linearization) expressed in form

$$\begin{aligned} R_{i,i+1} &= \frac{1}{2}\grave{\boldsymbol{c}}_i^T \boldsymbol{B}_{e_i}\grave{\boldsymbol{c}}_i = \frac{1}{2}\boldsymbol{c}_i^T \underbrace{\boldsymbol{\tau}_{\alpha_i}^T \boldsymbol{B}_{e_i}\boldsymbol{\tau}_{\alpha_i}}_{\tilde{\boldsymbol{B}}_{e_i}} \boldsymbol{c}_i = \frac{1}{2}\boldsymbol{c}_i^T\tilde{\boldsymbol{B}}_i\boldsymbol{c}_i \\ &= \frac{1}{2}\left(\boldsymbol{\tau}_{FB}\dot{\boldsymbol{q}}_{C_i} - \boldsymbol{\tau}_{FA}\dot{\boldsymbol{q}}_{C_{i+1}}\right)^T \tilde{\boldsymbol{B}}_{e_i}\left(\boldsymbol{\tau}_{FB}\dot{\boldsymbol{q}}_{C_i} - \boldsymbol{\tau}_{FA}\dot{\boldsymbol{q}}_{C_{i+1}}\right). \end{aligned} \tag{39}$$

The complete dissipation energy of all damping elements is then

$$R = \sum_{i=1}^{60} R_{i,i+1} = \sum_{i=1}^{60}\left(\frac{1}{2}\dot{\boldsymbol{q}}_{C_i}^T\boldsymbol{\tau}_{FB}^T\tilde{\boldsymbol{B}}_{e_i}\boldsymbol{\tau}_{FB}\dot{\boldsymbol{q}}_{C_i} - \dot{\boldsymbol{q}}_{C_i}^T\boldsymbol{\tau}_{FB}^T\tilde{\boldsymbol{B}}_i\boldsymbol{\tau}_{FA}\dot{\boldsymbol{q}}_{C_{i+1}} + \frac{1}{2}\dot{\boldsymbol{q}}_{C_{i+1}}^T\boldsymbol{\tau}_{FA}^T\tilde{\boldsymbol{B}}_{e_i}\boldsymbol{\tau}_{FA}\dot{\boldsymbol{q}}_{C_{i+1}}\right) \tag{40}$$

where $\dot{\boldsymbol{q}}_{C_{61}} = \dot{\boldsymbol{q}}_{C_1}$.

After multiplying the previous equation and from identity $\frac{\partial R_{i,i+1}}{\partial \dot{\boldsymbol{q}}_R} = \boldsymbol{B}_{e_i}^{(R)}\dot{\boldsymbol{q}}_R$, we obtain the matrix of equivalent damping between two adjacent blades $i$ and $i+1$ in rotating global coordinate system in the form

$$\mathbf{B}_{e_i}^{(R)} = \begin{array}{c} \begin{array}{ccccc} & \boldsymbol{q}_{C_i}^T & & \boldsymbol{q}_{C_{i+1}}^T & \end{array} \\ \left[\begin{array}{c|c|c|c|c} \vdots & & \vdots & & \vdots \\ \hline \cdots & \tau_{FB}^T\tilde{\mathbf{B}}_{e_i}\boldsymbol{\tau}_{FB} & \cdots & -\tau_{FB}^T\tilde{\mathbf{B}}_{e_i}\boldsymbol{\tau}_{FA} & \cdots \\ \hline \vdots & & \vdots & & \vdots \\ \hline \cdots & -\boldsymbol{\tau}_{FA}^T\tilde{\mathbf{B}}_{e_i}\boldsymbol{\tau}_{FB} & \cdots & \boldsymbol{\tau}_{FA}^T\tilde{\mathbf{B}}_{e_i}\boldsymbol{\tau}_{FA} & \cdots \\ \hline \vdots & & \vdots & & \vdots \end{array}\right] \end{array} \begin{array}{l} \\ \\ \boldsymbol{q}_{C_i} \\ \\ \boldsymbol{q}_{C_{i+1}} \\ \\ \end{array} \begin{array}{l} \left.\begin{array}{c} \\ \\ \end{array}\right\} \boldsymbol{q}_{B,i} \\ \left.\begin{array}{c} \\ \\ \end{array}\right\} \boldsymbol{q}_{B,i+1} \end{array}, \tag{41}$$

where $\boldsymbol{q}_{B,i}$ and $\boldsymbol{q}_{B,i+1}$ are the vectors of all generalized displacements of blade $i$-th and $i+1$-th. Vectors $\boldsymbol{q}_{C_i}$ and $\boldsymbol{q}_{C,i+1}$ are the vectors of generalized displacements in the last node $N$ on blade $i$ and $i$-th, respectively.

Because the individual matrices $\tilde{\boldsymbol{B}}_{e_i}^{(R)}$ have different calculation (see below), the whole matrix of equivalent damping between all blades is then for 60 blades

$$
\begin{array}{cc}
 & \begin{array}{ccccccc} \phantom{\cdots} & \boldsymbol{q}_{C_1}^T & \phantom{\cdots} & \boldsymbol{q}_{C_2}^T & \phantom{\cdots} & \boldsymbol{q}_{C_3}^T & \phantom{\approx} \end{array} \\
\mathbf{B}_e^{(R)} = & \left[\begin{array}{c|c|c|c|c|c|c}
\vdots & & \vdots & & \vdots & & \vdots \\ \hline
\cdots & \tau_{FB}^T\tilde{\mathbf{B}}_{e_1}\boldsymbol{\tau}_{FB} + \tau_{FA}^T\tilde{\mathbf{B}}_{e_{60}}\boldsymbol{\tau}_{FA} & \cdots & -\tau_{FB}^T\tilde{\mathbf{B}}_{e_1}\boldsymbol{\tau}_{FA} & \cdots & & \approx \\ \hline
\vdots & & \vdots & & \vdots & & \vdots \\ \hline
\cdots & -\boldsymbol{\tau}_{FA}^T\tilde{\mathbf{B}}_{e_1}\boldsymbol{\tau}_{FB} & \cdots & \tau_{FA}^T\tilde{\mathbf{B}}_{e_1}\boldsymbol{\tau}_{FA} + \tau_{FB}^T\tilde{\mathbf{B}}_{e_2}\boldsymbol{\tau}_{FB} & \cdots & -\tau_{FB}^T\tilde{\mathbf{B}}_{e_2}\boldsymbol{\tau}_{FA} & \approx \\ \hline
\vdots & & \vdots & & \vdots & & \vdots \\ \hline
\cdots & & \cdots & -\boldsymbol{\tau}_{FA}^T\tilde{\mathbf{B}}_{e_2}\boldsymbol{\tau}_{FB} & \cdots & \tau_{FB}^T\tilde{\mathbf{A}}_{e_2}\boldsymbol{\tau}_{FA} + \tau_{FB}^T\tilde{\mathbf{B}}_{e_3}\boldsymbol{\tau}_{FB} & \approx \\ \hline
\approx & \approx & \approx & \approx & \approx & \approx & \approx \\
\approx & \approx & \approx & \approx & \approx & \approx & \approx \\ \hline
\vdots & & \vdots & & \vdots & & \vdots \\ \hline
\cdots & & \cdots & & \cdots & & \approx \\ \hline
\vdots & & \vdots & & \vdots & & \vdots \\ \hline
\cdots & -\tau_{FB}^T\tilde{\mathbf{B}}_{e_{60}}\boldsymbol{\tau}_{FA} & \cdots & & \cdots & & \approx
\end{array}\right].
\end{array}
\tag{42}
$$

After this step, the equation of motion (31) can be completed by equivalent damping matrix obtained from previous equation

$$
\boldsymbol{M}\ddot{\boldsymbol{q}}(t) + (\boldsymbol{B}_e + \omega\boldsymbol{G})\,\dot{\boldsymbol{q}}(t) + \left(\boldsymbol{K}_s + \omega^2\boldsymbol{K}_\omega - \omega^2\boldsymbol{K}_d\right)\boldsymbol{q}(t) = \boldsymbol{f}(t), \tag{43}
$$

where

$$
\boldsymbol{B}_e = diag(\mathbf{0} \quad \boldsymbol{B}_e^{(R)}). \tag{44}
$$

The algorithm of $\tilde{\boldsymbol{B}}_{e_i}$ and $\boldsymbol{B}_e^{(R)}$ calculation is

- Calculate of the vector of complex amplitudes $\tilde{\boldsymbol{q}}$ as a response on the acting forces using model (43) with equivalent damping (for first iteration is $\boldsymbol{B}_e = \mathbf{0}$).
- Find the axes of movement ellipse for every damping element and the angle of ellipse rotation, e.g. $b_i$, $a_i$ and $\alpha_i$ for $i = 1, 2, \ldots, r$, where $r$ is number of blades, i.e. number of damping elements in shroud. The formula is:
  - $b_i = |\boldsymbol{\xi}_B^T\tilde{\boldsymbol{q}}_{C_i} - \boldsymbol{\xi}_A^T\tilde{\boldsymbol{q}}_{C_{i+1}}|$,
  - $a_i = |\boldsymbol{\eta}_B^T\tilde{\boldsymbol{q}}_{C_i} - \boldsymbol{\eta}_A^T\tilde{\boldsymbol{q}}_{C_{i+1}}|$,
  - $\alpha_i = |\boldsymbol{\zeta}_B^T\tilde{\boldsymbol{q}}_{C_i} - \boldsymbol{\zeta}_A^T\tilde{\boldsymbol{q}}_{C_{i+1}}|$.
- Calculate the elements $b_{\xi_i}$, $b_{\hat{\eta}_i}$ and $b_{\Phi_i}$ of matrices $\boldsymbol{B}_i$:
  - $b_{\xi_i} = \frac{4T}{\pi a_i \omega_k}$,
  - $b_{\hat{\eta}_i} = \frac{4T}{\pi b_i \omega_k}$,
  - $b_{\Phi_i} = \frac{4M}{\pi \Phi_i \omega_k}$.
- From previous results the local equivalent damping matrix of $i$-th element is

$$
\tilde{\boldsymbol{B}}_{e_i} = \begin{bmatrix} b_{\xi_i}\cos^2\alpha_i + b_{\hat{\eta}_i}\sin^2\alpha_i & (b_{\xi_i} - b_{\hat{\eta}_i})\cos\alpha_i\sin\alpha_i & 0 \\ (b_{\xi_i} - b_{\hat{\eta}_i})\cos\alpha_i\sin\alpha_i & b_{\xi_i}\sin^2\alpha_i + b_{\hat{\eta}_i}\cos^2\alpha_i & 0 \\ 0 & 0 & b_{\Phi_i} \end{bmatrix}. \tag{45}
$$

- Assemble the global equivalent damping matrix of friction forces in shroud $\boldsymbol{B}_e^{(R)}$.
- Rerun whole algorithm with $\boldsymbol{B}_e^{(R)}$ placed in (43) until the solution results don't converge.

The friction force $T$ is defined by damping element normal force $N_0$ induced by centrifugal load and by friction coefficient $f$: $T = N_0 f$, the friction moment $M = \frac{2}{3} f r_{ef} N_0$, where $r_{ef}$ is the effective radius of friction moment.

The forces acting on blades are induced by steam flow fluctuations caused by nozzles (stationary blades). The frequency of this harmonic load is $\omega_k = \omega * n_S$, where $n_S$ is the number of nozzles. That's why the rotating blade passes $n_S$ fluctuations per revolute, which can be approximate by sinusoidal force. This force has axial $F_{ax}$ and tangential $F_{tan}$ components, whereas the phase delay angle between these components is $\varphi$ and can be obtained from CFD analysis. The forces acting on the blade are assumed to identical in every blade node, i.e. $F_{ax_{ij}} = F_{ax_{ij+1}}$, where $i$ is blade index, $i \in 1, 2, \ldots, r$ and $j$ is index of blade node, $j \in 1, 2, \ldots, N$.

$$\begin{aligned} F_{ax_{1j}} &= F_{ax}\cos(\omega_k t), & F_{tan_{1j}} &= F_{tan}\cos(\omega_k t - \varphi), \\ F_{ax_{2j}} &= F_{ax}\cos(\omega_k (t + \triangle t)), & F_{tan_{2j}} &= F_{tan}\cos(\omega_k (t + \triangle t) - \varphi), \\ F_{ax_{ij}} &= F_{ax}\cos(\omega_k (t + (i-1)\triangle t)), & F_{tan_{ij}} &= F_{tan}\cos(\omega_k (t + (i-1)\triangle t) - \varphi), \end{aligned} \tag{46}$$

where $\triangle t$ is the time delay of passing adjacent blades around the same nozzle. This time delay is equal $\frac{2\pi}{r\omega}$, where $\omega$ is the angular speed of bladed disk rotation. Using $\omega = \omega_k / n_s$, the equations in (46) can be expressed as

$$F_{ax_{ij}} = F_{ax}\cos(\omega_k t + \underbrace{(i-1)\omega_k \frac{2\pi}{r\omega}}_{\varphi_i}), \quad F_{tan_{ij}} = F_{tan}\cos(\omega_k t + \underbrace{(i-1)\omega_k \frac{2\pi}{r\omega} - \varphi}_{\psi_i = \varphi_i - \varphi}), \tag{47}$$

i.e. in complex form

$$\tilde{F}_{ax_{ij}} = F_{ax} e^{\omega_k t + \varphi_i}, \qquad \tilde{F}_{tan_{ij}} = F_{tan} e^{\omega_k t + \psi_i}. \tag{48}$$

The complex vector of one blade excitation is then

$$\tilde{\boldsymbol{f}}_i(t) = \tilde{\boldsymbol{f}}_i e^{i\omega_k t} \tag{49}$$

where

$$\tilde{\boldsymbol{f}}_i = F_{ax}\,[0\;1\;0\;0\;0\;0\ldots0\;1\;0\;0\;0\;0\ldots]^T\, e^{i\varphi_i} - F_{tan}\,[0\;0\;1\;0\;0\;0\ldots0\;0\;1\;0\;0\;0\ldots]^T\, e^{i\psi_i}. \tag{50}$$

The nonzeros elements express the existing actuating force component, in first bracket it is in the axial direction (second DOF of every node), in second bracket it is in tangetial direction (third DOF of every node). The complex force vector of the whole blade rim, respectively bladed disk, is then

$$\tilde{\boldsymbol{f}}_R(t) = \begin{bmatrix} \tilde{\boldsymbol{f}}_1^T & \tilde{\boldsymbol{f}}_2^T & \ldots \tilde{\boldsymbol{f}}_r^T \end{bmatrix} e^{i\omega_k t}, \quad \text{resp.} \quad \boldsymbol{f}(t) = [\mathbf{0}^T \quad \tilde{\boldsymbol{f}}_R^T] e^{i\omega_k t}. \tag{51}$$

The results for fourth iteration of forced vibration follows. The system of bladed disk with damping elements is in shroud coupled together by coupling stiffness matrix $\mathbf{K}_C^{(R)}$ in normal direction to contact area (that's why the tangential displacements of shrouds in fig. 11 are "smooth"), but in other DOF can slip occur (see axial displacements of shrouds in fig. 10). The forced vibration in time are displayed in fig. 12 and 13.

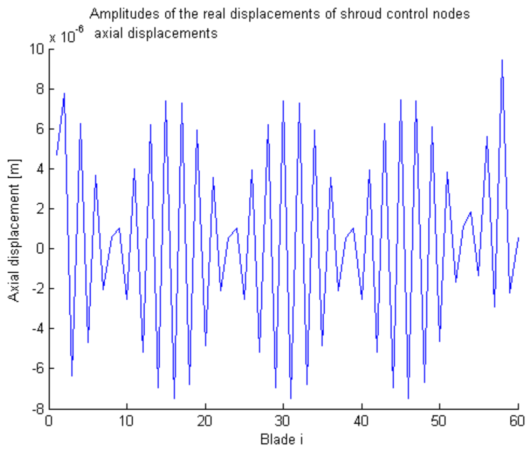


Obrázek 10: Amplitudes of the real displacements of shroud control nodes $C_i$ in axial direction.

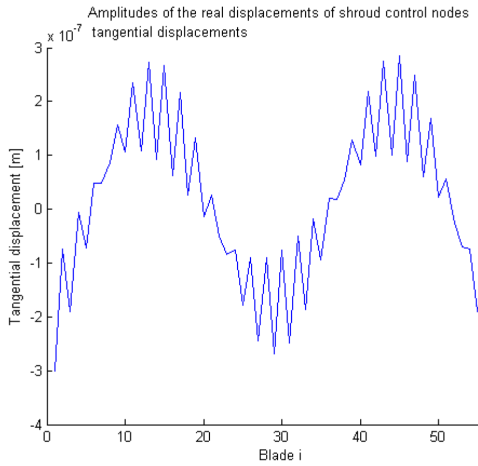


Obrázek 11: Amplitudes of the real displacements of shroud control nodes $C_i$ in tangential direction.

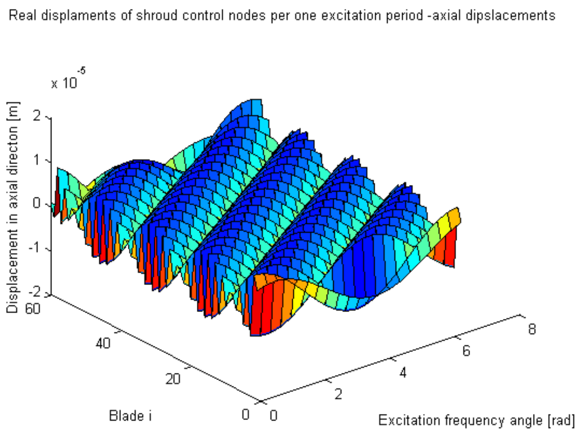


Obrázek 12: Real displacements of shroud control nodes in axial direction per excitation frequency angle.

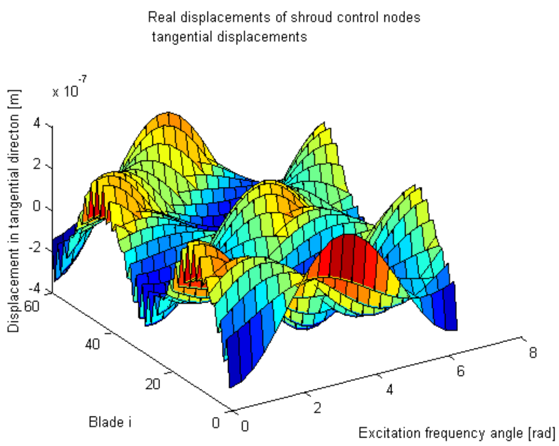


Obrázek 13: Real displacements of shroud control nodes in tangential direction per excitation frequency angle.

## 7. Conclusion

The presented method and the corresponding developed software enables to create small computational consuming model of the bladed disk for nonlinear task. The disk is modelled as a three dimensional rotating continuum and blades as a one dimensional continuum with rigid shroud connected by damping elements. The displacements of the coupled disk nodes on the rigid blade foots are eliminated by means of displacements in the first blade nodes. The contact stiffnesses of a damping elements supported between blade shroud are respected in sliding interface surfaces. In presented stage of modelling the contact surfaces are considered as smooth. The method allows to introduce continuously distributed centrifugal and gyroscopic effects which influence the bladed disk modal properties. Modal values of particular components of the complete model were compared with modal values calculated using commercial software. The modal accurance is good. For including the friction effects of damping elements in shroud, an equivalent linearization method is used for creation the equivalent damping matrix and the forced vibration analysis is introduced. The model doesn't use the cyclic symmetry and is prepared for system with different blades (with and without shroud). In future, the input parameters can be specified by collateral detailed analysis of two blades with one damping element and from experiment.

The new approach to bladed disk vibration modelling was tested for undamped modeled bladed disk with sixty blades and damping elements. From a modal analysis follows that the developed software in MATLAB code based on presented methodology is acceptable for a modelling of damping effects.

## 8. Acknowledgment

This work was supported by GA CR in the project No. 101/09/1166 "Research of the dynamic behaviour and optimization of complex rotating system with non-linear couplings and high damping materials" and the research project MSM 49 777 513 03 supported by the Ministry of Education, Youth and Sports of the Czech Republic.

## 9. Reference

Šašek, J. & Hajžman, M. 2006: Modal properties of rotating disks. *Proceedings of the 22nd Computational Mechanicss*, Vol2, pp. 593-600.

Kellner, J. & Zeman, V. 2006: Infuences of dynamic stiffnes, centrifugal forces and blade's elastic seating on blade modal properties, *Proceedings of the 8th Applied Mechanics* , pp. 47-48.

Zeman, V. & Šašek, J. & Byrtus, M. 2009: Modelling of rotating disk vibration with fixed blades, *Modelling and optimization of physical systems 8* , pp125-130.

Rao, S., S. 1989: *The finite element method of engineering*.

Kellner, J. 2009: *Vibration of turbine blades and bladed disks (in Czech)*, Doctoral thesis.

Riwin, E., I. 1999: *Stiffness and damping in mechanical design*.